



Article

Numerical Simulation Approach for a Dynamically Operated Sorption-Enhanced Water-Gas Shift Reactor

Tabea J. Stadler ¹, Jan-Hendrik Knoop ¹, Simon Decker ² and Peter Pfeifer ^{1,*}¹ Institute for Micro Process Engineering (IMVT), Karlsruhe Institute of Technology (KIT), Hermann-von-Helmholtz-Platz 1, 76344 Eggenstein-Leopoldshafen, Germany² Elektrotechnisches Institut (ETI), Karlsruhe Institute of Technology (KIT), Kaiserstr. 12, 76131 Karlsruhe, Germany

* Correspondence: peter.pfeifer@kit.edu

Abstract: A dynamically operated sorption-enhanced water–gas shift reactor is modelled to leverage its performance by means of model-based process design. This reactor shall provide CO₂-free synthesis gas for e-fuel production from pure CO. The nonlinear model equations describing simultaneous adsorption and reaction are solved with three numerical approaches in MATLAB: a built-in solver for partial differential equations, a semi-discretization method in combination with an ordinary differential equation solver, and an advanced graphic implementation of the latter method in Simulink. The novel implementation in Simulink offers various advantages for dynamic simulations and is expanded to a process model with six reaction chambers. The continuous conditions in the reaction chambers and the discrete states of the valves, which enable switching between reactive adsorption and regeneration, lead to a hybrid system. Controlling the discrete states in a finite-state machine in Stateflow enables automated switching between reactive adsorption and regeneration depending on predefined conditions, such as a time span or a concentration threshold in the product gas. The established chemical reactor simulation approach features unique possibilities in terms of simulation-driven development of operating procedures for intensified reactor operation. In a base case simulation, the sorbent usage for serial operation with adjusted switching times is increased by almost 15%.

Keywords: sorption-enhanced water–gas shift (SEWGS); reactor modeling; nonlinear hybrid dynamic system simulation; method-of-lines (MoL); pdepe solver; MATLAB Simulink Stateflow



Citation: Stadler, T.J.; Knoop, J.-H.; Decker, S.; Pfeifer, P. Numerical Simulation Approach for a Dynamically Operated Sorption-Enhanced Water-Gas Shift Reactor. *Processes* **2022**, *10*, 1160. <https://doi.org/10.3390/pr10061160>

Academic Editors: Liming Dai and Jialin Tian

Received: 19 May 2022

Accepted: 7 June 2022

Published: 9 June 2022

Publisher's Note: MDPI stays neutral with regard to jurisdictional claims in published maps and institutional affiliations.



Copyright: © 2022 by the authors. Licensee MDPI, Basel, Switzerland. This article is an open access article distributed under the terms and conditions of the Creative Commons Attribution (CC BY) license (<https://creativecommons.org/licenses/by/4.0/>).

1. Introduction

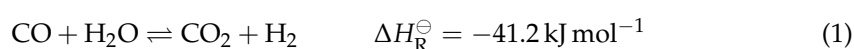
In November 2021, the participants of the Conference of the Parties COP26 in Glasgow agreed on a stronger commitment to the aims set in the Paris Agreement back in 2015: reducing the limitation of global warming to 1.5 °C [1,2]. To reach this ambitious goal, anthropogenic greenhouse gas emissions must be drastically reduced. Potential for reduction is especially possible in the transport sector, where fossil fuels must be replaced by sustainable alternatives. A promising substitute in the case of aviation is synthetic jet fuel produced in so-called Power-to-Liquid processes [3].

Such a process is developed in the Kerogreen project. In this project, a container-sized pilot plant is being built, in which captured CO₂, H₂O, and renewable energy are converted to the target product kerosene [4]. One unit operation within the process chain comprises a compact sorption-enhanced water–gas shift (SEWGS) reactor. Here, purified CO from a plasma reactor is partly converted with steam to produce hydrogen. Two main targets are pursued in this process step:

1. Providing synthesis gas (syngas) with a H₂/CO ratio of approximately two for the subsequent Fischer–Tropsch synthesis.
2. Removing the by-product CO₂ and refeeding it to the plasma reactor.

In sorption-enhanced reactors, or, in other words, *adsorptive reactors*, a chemical reaction and an adsorptive separation of one product component are carried out simultaneously [5]. Simultaneous reaction and adsorption usually take place in fixed bed reactors filled with solid catalyst and sorbent material.

In our case of the SEWGS reactor, the exothermic water–gas shift reaction (WGS, Equation (1)) on a Cu-based catalyst is combined with in-situ adsorption of CO₂ on a potassium-impregnated hydrotalcite sorbent (K-HTC). Many experimental studies have proven the feasibility of this technology [6–8]; a comprehensive overview is given in [9]. According to Le Chatelier’s principle, the selective removal of the product component CO₂ (Equation (2)) shifts the reaction equilibrium towards the product side. Hence, higher yields of the desired product component H₂ can be obtained, and the undesired product component CO₂ can be recycled. Depending on prevailing operating conditions, H₂O is also adsorbed on K-HTC (Equation (3)).



Due to its limited adsorption capacity, the sorbent gets saturated with adsorbate during the reactive adsorption phase and needs to be regenerated for further use. Regeneration can either be realized by temperature swing (temperature swing adsorption, TSA), pressure swing (pressure swing adsorption, PSA), or a combination thereof (PTSA) and is often stimulated by a concentration change (purge flow). The adsorption capacity of the sorbent is lowered by changing the prevailing process conditions: increasing the temperature or decreasing the pressure releases the adsorbate from the sorbent. To ensure continuous flow and concentration of product gas, several (at least two) parallel reactors must be operated in periodically switching modes: at least one in reactive adsorption mode and one (or more) in regeneration (desorption) mode [10]. Usually, the required regeneration time is longer than the time span of reactive adsorption. Hence, sorption-enhanced reactor systems consist of multiple (about six to nine) equivalent reactors [11], which are operated in periodically switching modes. Depending on the process concept, these modes may include for a PSA:

- pressurization (feed: reactants);
- reactive adsorption (feed: reactants);
- depressurization (no feed, often purged);
- regeneration (feed: purge gas).

A periodic reactive adsorption and regeneration cycle consists of a consecutive sequence of all relevant steps and is repeated continuously. To enhance performance and efficiency, ideal operating conditions for periodic cycles must be ensured.

Modeling and simulation techniques are precious tools to develop optimized process strategies. They aim to perform simulative parameter studies based on sorption-enhanced reactor models to gather deeper understanding of the interior states of the reactor system. Several approaches for reactive adsorption models were developed over the last years, and detailed studies on the intrinsic adsorption and reaction behavior are available for specific applications.

Sorption-enhanced processes are time- and space-dependent and can be described by a system of coupled partial differential equations (PDE). Although single PDEs might be solved analytically, numerical solvers are needed to compute coupled PDEs. Besides the complex and time-consuming development of a customised solving algorithm for a special problem, more general commercial numeric tools, such as built-in solvers in MATLAB (The MathWorks Inc., USA), COMSOL Multiphysics (COMSOL Inc., Sweden), or gPROMS (Siemens PSE, UK) are available for solving PDE systems. Furthermore, semi-discretization methods (Method-of-Lines, MoL) can be used to transform a PDE into a system of ordinary differential equations (ODE) [12], which can then be solved by well-established ODE

solving algorithms. Table 1 gives a short overview of selected studies employing those methods for (reactive) adsorption processes.

Table 1. Overview of selected studies employing different numerical methods for solving (reactive) adsorption models.

Reaction	Adsorption	Numerical Solution	Reference
-	CO ₂ on K-HTC	MATLAB: MoL (N = 500) / ode15s solver	[13]
SMR	CO ₂ on K-HTC	MATLAB: MoL / ode15s solver	[14]
WGS	CO ₂ on K-HTC	gPROMS: CFDM (N = 600) / DASOLV solver	[15]
WGS	CO ₂	COMSOL Multiphysics: FEM	[16]
SMR	CO ₂ on CaO-mayenite	MATLAB: pdepe solver	[17]
DMES	H ₂ O on LTA zeolite	MATLAB: MoL (N = 30) / ode15s solver	[18]
DMES	H ₂ O on LTA zeolite 3A	gPROMS: BFDM (N = 60) / DASOLV solver	[19,20]
WGS	CO ₂ on K-HTC	MATLAB: MoL (N = 250) / ode15s solver	[21]
SMR	CO ₂ on CaO	MATLAB: pdepe solver	[22]
-	CO ₂ on K-HTC	gPROMS	[23]

Whereas most studies focus on the model description of simultaneous adsorption and reaction in one reactor, the dynamic modeling of multiple interconnected reactors has received less attention. Only few studies have investigated full-cycle behavior [15,16,18,23,24].

Najmi et al., for example, developed a multi-train SEWGS model that consists of eight parallel reactors [15]. They implemented a set of PDEs describing reactive adsorption, regeneration, and various PSA process cycle steps in gPROMS (axial discretization in 600 elements by centered finite difference method (CFDM), time integration by DASOLV solver) and created an operating schedule that switches the set of equations between reactive adsorption and desorption after defined cycle times.

Recently, van Kampen et al. presented an elaborated model study on the sorption-enhanced dimethyl-ether synthesis, in which they demonstrated a full-cycle design for a three column PTSA system [18]. The numerical solution was realized by means of spatial discretization according to MoL with 30 finite differences (FD) and time integration with MATLAB ode15s solver for pre-defined time spans of reactive adsorption/regeneration steps.

In this contribution, we apply a novel numerical solution approach that has not been described previously for dynamic sorption-enhanced reactor modeling. It is based on the graphical implementation of the ODE system obtained via MoL in the MATLAB Simulink programming environment. Simulink enables the implementation and analysis of the SEWGS reactor as a dynamic system. The cyclic process operation procedure is implemented with the Simulink add-on Stateflow. Stateflow is a tool to create state-machines and flow-charts in Simulink. With Simulink and Stateflow, the hybrid system consisting of parallel and periodically operated fixed beds and the discrete switches between different modes can be fully described.

With this model, switching times for reactive adsorption and regeneration no longer need to be predefined. Instead, they can be adjusted automatically during run time according to a defined threshold, e.g., the CO₂ content in the reaction chamber outlet.

2. SEWGS Model

2.1. Model Development

A one-dimensional, time- and space resolved dynamic reactor model was developed to investigate numerical approaches and process configurations. The packed bed reactor dimensions and operating conditions were chosen in accordance with the pilot plant reactor in the Kerogreen project. This reactor consists of six individually fed reaction chambers embedded in one diffusion-bonded apparatus (Figure 1).

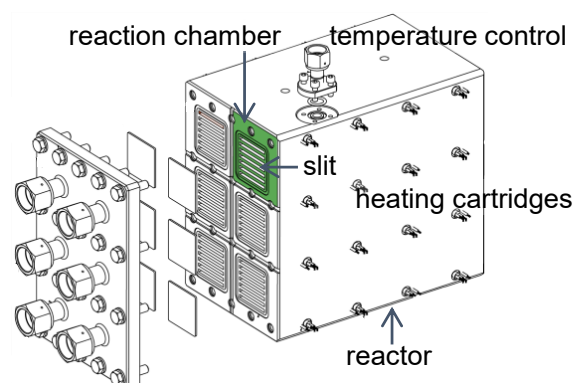


Figure 1. Pilot plant SEWGS reactor with six individually fed reaction chambers. Every chamber consists of seven slits. Isothermal conditions are ensured with adjacent channels between the slits for tempering with purge gas.

In cyclic operation, the chambers can be operated in parallel or in series: the outlet of one reaction chamber can be coupled with the inlet of the next reaction chamber for a serial configuration. Each reaction chamber consists of seven rectangular slits ($h = 4$ mm, $w = 50$ mm, $l = 300$ mm). The slits are filled with a homogeneous mixture of K-HTC and Cu/ZnO-Al₂O₃ catalyst particles. Due to the rather low adsorption capacity of K-HTC, the SEWGS reactor in the Kerogreen pilot plant employs a PSA concept with fast switching times for continuous H₂ production. Contrary to concepts with large, thick vessels as reactor compartments, where severe back-mixing can occur, the slits are assumed to behave like ideal plug flow reactors.

The SEWGS reactor merges several elements of process intensification [25,26]. In terms of processing methods, it can be classified as a multi-functional reactor for dynamically operated reactive separation processes. In terms of equipment, the SEWGS reactor exhibits excellent heat transfer properties due to adjacent tempering micro-channels between the slits that basically form a micro heat-exchanger and enable isothermal operation conditions in the reaction chambers. Sending purge gas (N₂ with steam) through the tempering channels prior to entering the chambers in desorption mode leads to a negligible temperature difference between adsorption and desorption slits. The model is based on the following assumptions and considerations:

- Homogeneous distribution of uniformly sized catalyst and sorbent particles according to their weight fraction assumed as one phase
- Uniform gas distribution in the reaction chambers
- Isothermal conditions in the slits
- Negligible pressure drop in the slits
- Constant superficial velocity (which is only the case for sufficient dilution, [27])
- No gradients rectangular to flow direction
- Axial dispersion considered with axial dispersion coefficient
- External mass transfer limitations neglected (Maers criterion)
- Internal mass transfer limitations considered (Weisz–Prater criterion) and implemented with linear driving force (LDF) model (Glueckauf criterion)
- WGS reaction [28] and simultaneous adsorption of CO₂ and H₂O on three different sorption sites (A: H₂O only, B: CO₂ only, C: H₂O and CO₂ comparatively) [29]
- Equilibrium-based desorption of H₂O and CO₂.

2.2. Model Equations

The mole balances for species $i = \text{CO}, \text{H}_2\text{O}, \text{CO}_2, \text{H}_2, \text{N}_2$ in the bulk gas phase are given in Equation (4). A heterogeneous LDF approximation was used for intraparticle mass transfer limitations to account for the porous character of the particles.

$$\varepsilon_b \frac{\partial c_i}{\partial t} = -u \frac{\partial c_i}{\partial z} + \varepsilon_b D_{ax,i} \frac{\partial^2 c_i}{\partial z^2} + (1 - \varepsilon_b) k_{LDF,i} (\bar{c}_i - c_i) \quad (4)$$

The required initial conditions are implemented according to the prevailing conditions in the reaction chambers before the switch (e.g., end of desorption mode before reactive adsorption) and the boundary conditions according to Equation (5) at the inlet (Dirichlet) and Equation (6) at the outlet (Neumann) of the reaction chambers. The initial conditions for the first reactive adsorption step result from a 2 h regeneration step to represent a fresh sorbent.

$$\text{at } z = 0 \quad c_i = c_{i,feed} \quad t > 0 \quad (5)$$

$$\text{at } z = 1 \quad \frac{\partial c_i}{\partial z} = 0 \quad t > 0 \quad (6)$$

The mole balances for species $i = \text{CO}, \text{H}_2\text{O}, \text{CO}_2, \text{H}_2, \text{N}_2$ in the particle void phase, where reaction and adsorption or desorption are assumed to take place on the solid surface, are given in Equation (7) for an axial dependent averaged particle concentration. The stoichiometric reaction coefficient ν_i is -1 for the reactants (CO and H₂O), 1 for the products (CO₂, H₂), and 0 for inert N₂. The adsorption rates of H₂O and CO₂ are given in Equation (8) and Equation (9), respectively. Initial conditions are defined analogous to the bulk phase.

$$\varepsilon_p \frac{\partial \bar{c}_i}{\partial t} = \varepsilon_p k_{LDF,i} (c_i - \bar{c}_i) + w_{cat} \rho \nu_i r_{WGS} - (1 - w_{cat}) \rho a_{ads,i} \quad (7)$$

$$a_{ads,H_2O} = \frac{\partial q_{A,H_2O}}{\partial t} + \frac{\partial q_{C,H_2O}}{\partial t} \quad (8)$$

$$a_{ads,CO_2} = \frac{\partial q_{B,CO_2}}{\partial t} + \frac{\partial q_{C,CO_2}}{\partial t} \quad (9)$$

The adsorption kinetics of adsorbate species H₂O and CO₂ on adsorption site A (H₂O only), B (CO₂ only), and C (H₂O and CO₂) of K-HTC sorbent are taken from Coenen et al. and are specified in Equation (10) (identical approach for q_{A,H_2O}) and Equation (11) (identical approach for q_{C,H_2O}), respectively [29]. The initial conditions are chosen according to the prevailing conditions in the reaction chambers before the switch.

$$\frac{\partial q_{B,CO_2}}{\partial t} = k_{B,ads} \cdot (q_{B,CO_2}^{eq} - q_{B,CO_2}) \quad \text{with} \quad q_{B,CO_2}^{eq} = k_B \cdot p_{CO_2}^{n_B} \quad (10)$$

$$\begin{aligned} \frac{\partial q_{C,CO_2}}{\partial t} &= k_{C,ads} \cdot p_{CO_2}^m \cdot (q_{C,max} - q_{C,H_2O} - q_{C,CO_2}) \\ &+ k_{C,rep1} \cdot q_{C,H_2O} \cdot p_{CO_2}^m - k_{C,rep2} \cdot q_{C,CO_2} \cdot p_{H_2O}^m - k_{C,des,CO_2} \cdot q_{C,CO_2} \end{aligned} \quad (11)$$

The desorption of site A and B was modelled with an equilibrium-dependent desorption coefficient (Equation (12), identical approach for q_{A,H_2O}). For site C, comparative replacement of CO₂ by H₂O takes place (Equation (11)). The heterogeneity of the surface is considered by a modified Elovich approach, shown for site B in Equation (13) (identical approach for site A and C) [29].

$$\frac{\partial q_{B,CO_2}}{\partial t} = k_{B,des} \cdot (q_{B,CO_2}^{eq} - q_{B,CO_2}) \quad (12)$$

$$k_{B,des} = k_{B,des}^1 \cdot \exp \left(- \frac{\left(-\beta_{B,des} \cdot \frac{q_{B,CO_2}}{q_{B,max}} \right)}{R \cdot T} \right) \quad (13)$$

The WGS reaction rate expression over a Cu/ZnO-Al₂O₃ catalyst is taken from Choi et al. and presented in Equation (14) [28]. The reaction equilibrium constant results from Equation (15) [30].

$$r_{\text{WGS}} = k_{\infty} \cdot \exp\left(-\frac{E_a}{R \cdot T}\right) \cdot \left(p_{\text{H}_2\text{O}} \cdot p_{\text{CO}} - \frac{p_{\text{H}_2} \cdot p_{\text{CO}_2}}{K_{\text{eq}}}\right) \quad (14)$$

$$K_{\text{eq}} = \exp\left(\frac{4577.8}{T} - 4.33\right) \quad (15)$$

The axial dispersion coefficient was determined with Equation (16) [19] with gas mixture diffusion coefficients from [31].

$$D_{\text{ax},i} = D_{\text{mix},i} \cdot \sqrt{\varepsilon_b} + u \cdot r_p \quad (16)$$

The linear driving force approximation coefficients were calculated according to Equation (17) [32] with effective diffusion coefficients from [31].

$$k_{\text{LDF},i} = \frac{15 \cdot D_{\text{eff},i}}{r_p^2} \quad (17)$$

2.3. Model Parameters

For the comparison of numerical solution approaches, a base case was investigated. The operating conditions and parameters for this base case are listed in Table 2. An overview of the kinetic coefficients is given in Appendix A, Table A1.

Table 2. Parameters and operating conditions used in the base case simulation.

General Parameters	
ε_b	0.4
ε_p	0.5
ρ	1096 kg m ⁻³
r_p	100 μm
w_{cat}	0.05
Adsorption Parameters	
p	8 bar
T	250 °C
F_{STP}	2000 mL/min
$y_{\text{CO,feed}}$	0.3
$y_{\text{H}_2\text{O,feed}}$	0.6
$y_{\text{N}_2,feed}$	0.1
Desorption Parameters	
p	1 bar
T	250 °C
F_{STP}	1000 mL/min
$y_{\text{H}_2\text{O,feed}}$	0.4
$y_{\text{N}_2,feed}$	0.6

3. Numerical Simulation Approaches

Three practical numerical simulation approaches for solving the SEWGS model are presented in the following sections. The simulations were performed on one core of the multi core processor Intel(R) Core(TM) i7-6700HQ CPU @ 2.60 GHz, with 8 GB of installed RAM memory using MATLAB version R2020b, 64-bit.

3.1. Built-In Solver

The system of coupled PDEs was solved with MATLAB's built-in solver pdepe for parabolic and elliptic PDEs in one dimension. This solver solves initial-boundary value problems in the form of Equation (18) with two independent variables: one spatial variable and time. The coefficients of Equation (18) have to be provided in the function handle pdefun, whereas initial and boundary conditions are specified in icfun and bcfun. The

boundary conditions must be coded according to Equation (19) [33]. At least one PDE must be parabolic. Therefore, the axial dispersion term in Equation (4) is required for the applicability of `pdepe` and the proper definition of boundary conditions.

$$c^* \left(z, t, v, \frac{\partial v}{\partial z} \right) \frac{\partial v}{\partial t} = z^{-m^*} \frac{\partial}{\partial z} \left(z^{m^*} f^* \left(z, t, v, \frac{\partial v}{\partial z} \right) \right) + s^* \left(z, t, v, \frac{\partial v}{\partial z} \right) \quad (18)$$

$$p^*(z, t, v) + q^*(z, t) f^* \left(z, t, v, \frac{\partial v}{\partial z} \right) = 0 \quad (19)$$

The `pdepe` solver transforms the system of PDEs into a system of ODEs by means of spatial discretization with a piecewise Petrov–Galerkin method on a set of user-defined nodes (`xmesh`) [34]. The resulting ODE system is integrated in time with the built-in solver `ode15s` for stiff differential algebraic equations (DAEs). DAEs arise from elliptic equations in the PDE system. The variable time step integration of `ode15s` delivers the numerical solution at specified points of time, defined in `tspan`. With this procedure, both time step and computing formula are adapted dynamically to obtain high accuracy in short computational time [35]. The `pdepe` solver provides a user-friendly implementation and is capable of solving nonlinear and coupled equations reliably for suitably defined meshes [36].

3.2. Method-of-Lines (MoL)

Another approach for solving coupled PDE systems is the MoL, a semi-discretization method [12]. Spatial derivatives in the PDEs are substituted by algebraic approximations to obtain a set of ODEs that can be solved with well-established solving algorithms. Here, spatial discretization is realized on a uniform grid in an axial direction (z -direction) with FD. For the first-order convective terms, a backward FD is used (Equation (20)), and for the second-order dispersion terms, implicit central differences are defined (Equation (21)). The resulting error O is neglected. The MoL resembles a CSTR cascade: with decreasing length of Δz , the number of cells N in the cascade increases and the error diminishes.

$$\frac{\partial v}{\partial z} \approx \frac{v_n - v_{n-1}}{\Delta z} + O(\Delta z) \quad \text{with} \quad n = 1, \dots, N \quad (20)$$

$$\frac{\partial^2 v}{\partial z^2} \approx \frac{v_{n+1} - 2v_n + v_{n-1}}{\Delta z^2} + O(\Delta z^2) \quad \text{with} \quad n = 1, \dots, N - 1 \quad (21)$$

The boundary conditions are implemented as differential equations on the first node ($n = 0$, Dirichlet), and on the last node ($n = N$, Neumann), analogous to Equation (5) and Equation (6) (*method of false boundaries*).

The obtained ODE system of $N + 1$ equations is numerically solved in time with MATLAB's `ode15s` for best comparability with the `pdepe` results. This variable-step, variable-order solver is based on numerical differentiation formulas and is recommended for stiff problems and DAEs. A convergence analysis with up to 250 cells is performed to examine the adequacy of the spatial discretization.

3.3. Simulink

Simulink is a graphical programming environment used for modeling, simulation, and analysis of dynamical systems that is based on MATLAB [37].

3.3.1. Model Implementation and Data Structure

In the third approach presented in this paper, the model equations are implemented in Simulink based on the idea of the MoL. In Simulink, the model is constructed in hierarchical block diagrams in the graphical editor, where libraries of predefined blocks of elementary model components for continuous-time and discrete-time systems are available [37]. Those blocks are connected with signal lines to visually build the model.

The SEWGS model equations are discretized in space to obtain ODEs for N cells, as described in Section 3.2. The ODEs are implemented in a block diagram as shown in

Figure 2 for the bulk concentration of CO [38]. Fourteen ODEs are needed to describe one cell (Figure 2). All ODEs of one cell have to be evaluated as a time-dependent single unit. Therefore, they are classified as one *atomic subsystem*. For simplified programming, the cell subsystem is stored in a separate file to be used multiple times as a *referenced subsystem* in the main model file, the so-called *parent model*. Ten subsequent cells are arranged in a *group* subsystem to enable easy scale-up and data storage. A reaction chamber comprises the desired number of groups in a cascade, as shown in Figure 2 for $N = 50$.

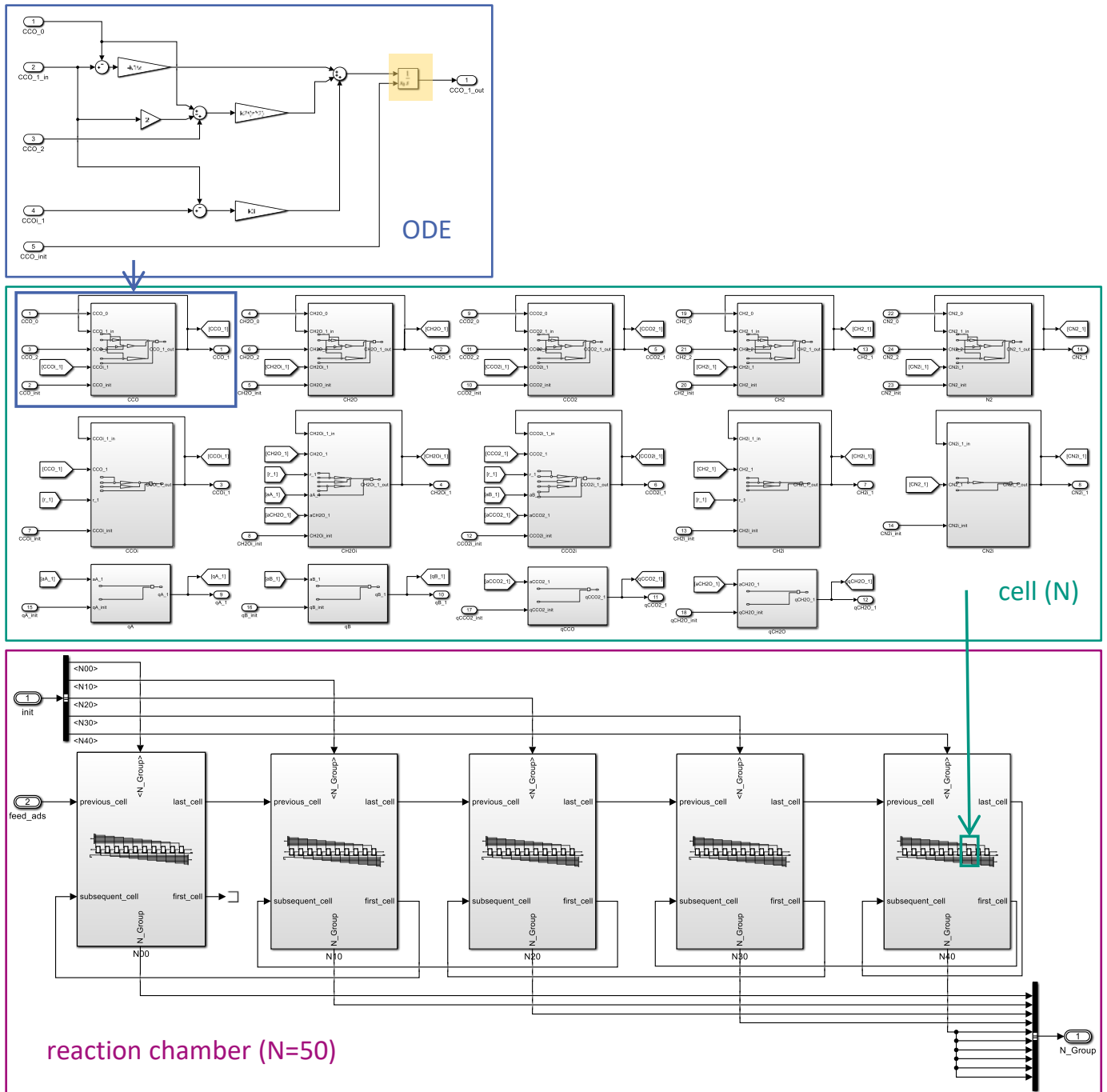


Figure 2. Bottom-up Simulink implementation of the model equations for one reaction chamber discretized analogous to MoL. Exemplary ODE implementation of the CO concentration in the bulk phase. The integrator block is marked in yellow. Fourteen ODEs arrange the cell subsystem; N (here: $N = 50$) cells form the reaction chamber.

The integrator block (marked in yellow in Figure 2) provides the selected solver (Section 3.3.2) with an initial condition that is used to compute the block's initial state at the start of the simulation and outputs the value of the integral of its time-dependent input signal at every time step.

A comprehensive *bus object* structure had to be developed for user-friendly and reliable data access. Simulink bus objects are equivalent to a structure definition in C. All relevant data belonging to one cell are stored together in one *cell bus object*. Ten cells are grouped in a superordinated *group bus object*. The desired number of groups form the whole reaction chamber and are contained in a *chamber bus object*. Each data point in every cell can easily be accessed via dot notation: e.g., the CO₂ concentration leaving the 25th cell is addressed as `N20.N05.CC02`. This structure simplifies data handling enormously, compared to the methods presented in Sections 3.1 and 3.2, where the overall time- and space dependent solution is contained in one voluminous matrix.

3.3.2. Solver Selection

The solver choice depends on the dynamics of the system, the solution stability, the solver robustness, and especially the computation speed when solving complex systems [39]. The different solvers suggested by the MATLAB solver library for ODEs were tested for the SEWGS model, with the aim to solve the model successfully within specified tolerance limits and in a reasonable duration. Figure 3 shows the required computation time for appropriate solvers depending on the implemented number of cells for the base case: reactive adsorption in one reaction chamber. Computation times below 0 indicate that a simulation did not converge, and a smaller error tolerance was required. With solver `ode23t`, the computation time was reduced by almost half compared to the commonly used solver `ode15s` with sufficient precision (relative error tolerance of 10^{-3}). This solver is used to speed-up all Simulink simulations presented in this paper.

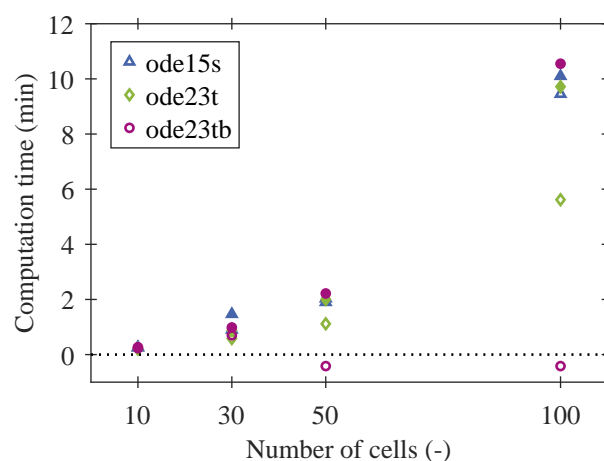


Figure 3. Required computation time depending on the number of implemented cells, chosen solver, and relative error tolerance. Filled symbols: relative error tolerance 10^{-6} ; open symbols: relative error tolerance 10^{-3} . The best results for $N = 100$ are obtained for solver `ode23t` with a relative error tolerance of 10^{-3} . Computation times below 0 indicate that a simulation did not converge.

3.3.3. Cyclic Process Design

A complex model, consisting of six parallel reaction chambers, is developed for continuous H₂ production. The automated switching logic from reactive adsorption to regeneration mode is realized with a finite-state-machine implemented in the Simulink tool Stateflow. Stateflow enables mode logic, fault management, and task scheduling in discrete or hybrid systems. A Stateflow machine contains Stateflow charts with objects such as states, events, transitions, etc. [40].

For the implemented periodic process, the valve positions (corresponding to the real plant) for either reactive adsorption or regeneration are triggered after an initialization step in all chambers by the Stateflow machine. One reaction chamber starts in reactive adsorption mode, while the other chambers are in regeneration mode. As soon as a specified event triggers the Stateflow machine, such as reaching a threshold concentration in the outlet flow or a predefined time span, the valve positions are changed in a way that the next reaction chamber starts its reactive adsorption period. A graphical overview of the SEWGS Simulink model is given in Figure 4.

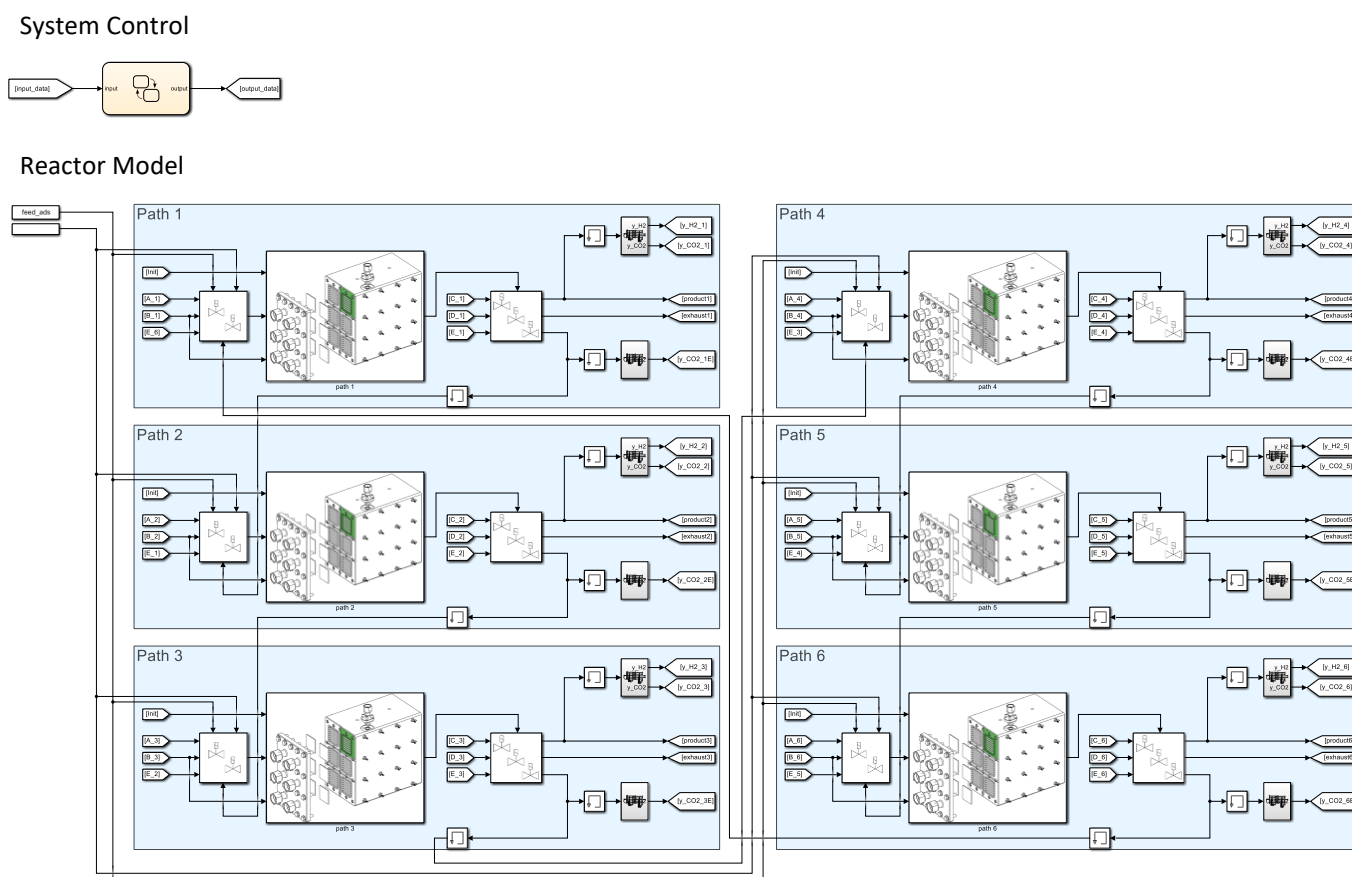


Figure 4. Simulink model consisting of six reaction chambers (blue), which are operated in either reaction or regeneration mode after an initialization step. Subsequent reaction chambers can optionally be connected. The cyclic process operation is controlled with a Stateflow machine (yellow).

In this paper, the dynamic adaptation of switching times depending on the CO_2 content in the reaction chamber outlet is investigated for a partly serial reaction chamber configuration.

4. Results and Discussion

In the following sections, the simulation results for reactive adsorption in one reaction chamber are compared for three numerical approaches. Furthermore, the cyclic process design for the SEWGS reactor consisting of six reaction chambers is presented.

4.1. Reactive Adsorption

The accuracy of the MoL simulations depends primarily on the adequacy of the grid discretization. In Figure 5a, the sorbent loading with CO_2 over the reactor length is shown for 10 to 250 cells at $t = 25$ s. The curves exhibit step steps for simulations with few cells, and the smoothness increases significantly for $N > 100$. The grid (in)dependence is

depicted in Figure 5b. For $N > 100$, the deviation from $N = 250$ is less than 5%, except for the initial conditions in the differently sized first cell.

The required computation time increased almost exponentially with the number of cells (see Appendix A, Table A2). Therefore, a trade-off between accuracy and computation time must be made, and $N = 100$ was chosen for the following MoL simulations.

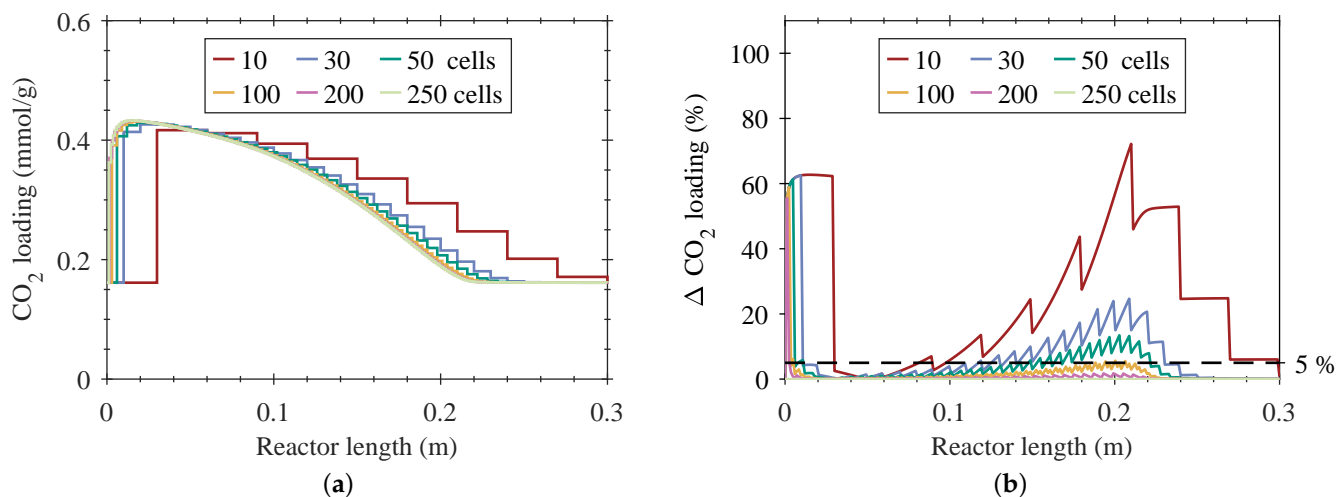


Figure 5. MoL grid analysis with $N = 10$ to 250 cells for reactive adsorption in one reaction chamber. (a) CO_2 loading, and (b) deviation of CO_2 loading from $N = 250$ as a function of the reactor length at $t = 25$ s.

The pdepe simulations have proven to be extremely sensitive to initial conditions. A sufficiently high number of mesh points in time and space needs to be chosen to ensure numerical stability and to avoid oscillations. The computation time for pdepe was significantly lower compared to MoL simulations with a comparable number of mesh points due to pdepe's run-time optimization (see Appendix A, Table A2). For both methods, MoL and pdepe, convergence could be reached with appropriate mesh settings.

In the base case, the CO_2 loading of the sorbent over the reactor length increases with time until it reaches full saturation after approximately 100 s (Figure 6a). At the same time, the CO_2 concentration at the reactor outlet approaches its steady-state value (Figure 6b). The defined breakthrough (CO_2 volume fraction in the product > 0.05) of CO_2 at the reactor outlet can be noticed after approximately 40 s. Prior to that point, CO is fully converted in excess of H_2O in the feed, and the produced CO_2 is adsorbed completely.

In order to assess the conservation properties of the numerical solution algorithms, the deviation from the molar balance depending on time and space was calculated (see Appendix A, Figure A1). Both methods, pdepe and MoL, exhibit only minor deviations from a closed molar balance ($< 2\%$). The deviation is more pronounced for pdepe close to the reactor inlet at $t < 50$ s. For MoL, the deviation emerges for a longer period of time at the reactor outlet. In both cases, it approaches zero as soon as steady-state conditions are reached. The deviations were attributed to the adsorption process and could—especially for undiluted feeds—possibly be improved by taking into account prevailing velocity changes, as suggested by DiGiuliano et al. [27].

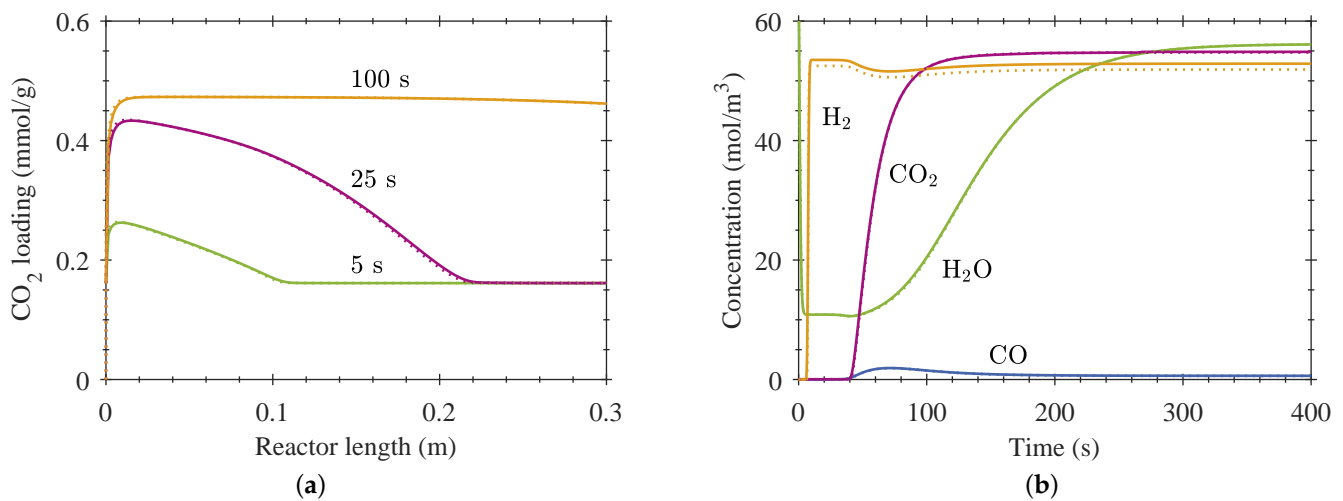


Figure 6. Comparison of pdepe and MoL ($N = 100$) simulation results for reactive adsorption in one reaction chamber. (a) CO₂ loading at various adsorption times as a function of the reactor length, and (b) bulk phase concentrations at reactor outlet as a function of time. Solid lines: MoL; dotted lines: pdepe.

After having shown that both approaches, pdepe as well as simple uniform semi-discretization with MoL, lead to satisfying results for the SEWGS simulation, the MoL results were compared with the corresponding Simulink results for $N = 100$. As expected, hardly any deviation between the curves of the two methods can be distinguished (Figure 7). Therefore, it was concluded that the graphical approach in Simulink performs with sufficient precision and reliability and can be expanded to a more complex hybrid process model.

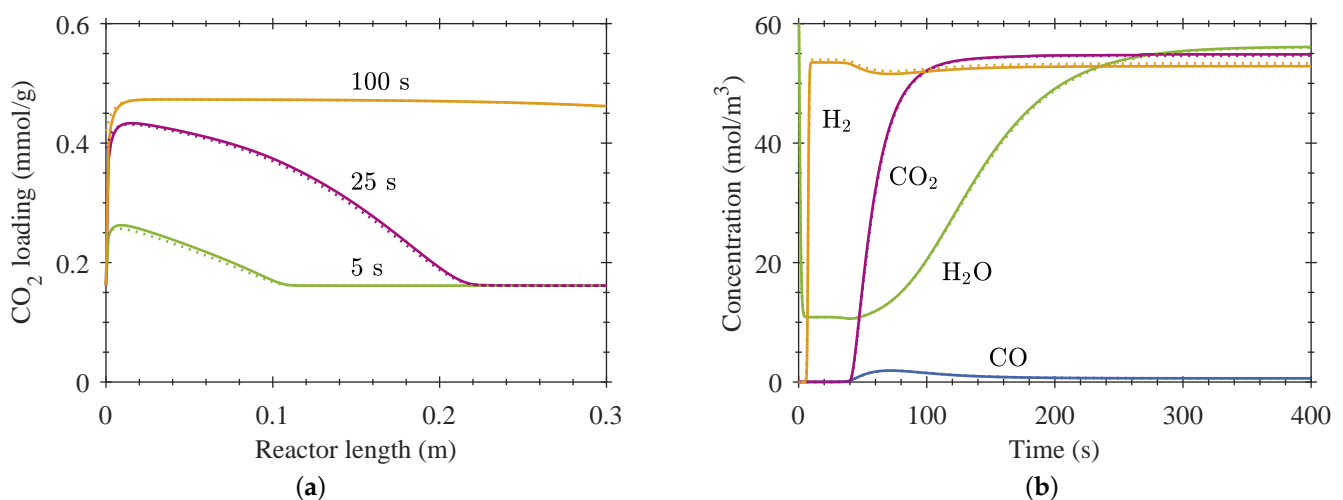


Figure 7. Comparison of MoL and Simulink ($N = 100$) simulation results for reactive adsorption in one reaction chamber. (a) CO₂ loading at various adsorption times as a function of the reactor length, and (b) bulk phase concentrations at reactor outlet as a function of time. Solid lines: MoL; dotted lines: Simulink ($N = 100$).

4.2. Process Design

The hybrid Simulink Stateflow model consisting of six reaction chambers, switching opportunities (valves), and process control (Stateflow machine) (Figure 4) is used to simulate cyclic SEWGS process operation. An interconnected reaction chamber configuration was investigated for optimized sorbent usage (Figure 8): chamber 1 starts in reactive adsorption mode (M2) with *fresh* feed (CO + H₂O) and produces CO₂-free WGS product, whereas all other chambers are in regeneration mode (M4). The regeneration feed consists

of N_2 and H_2O to increase CO_2 desorption from both sorption sites (B and C). As soon as the sorbent in chamber 1 is no longer capable of adsorbing all produced CO_2 and the gas flow leaving chamber 1 reaches a CO_2 volume fraction of 5%, a switch to M3 is triggered. In M3, the gas flow leaving chamber 1 is fed into chamber 2, which is then in M1. While the sorbent loading in chamber 1 is still increasing, CO_2 -free WGS product is produced in chamber 2. Chamber 1 switches from M3 to M4 when a threshold of 20% CO_2 volume fraction is reached. The cycle then continues in chamber 2 with M2.

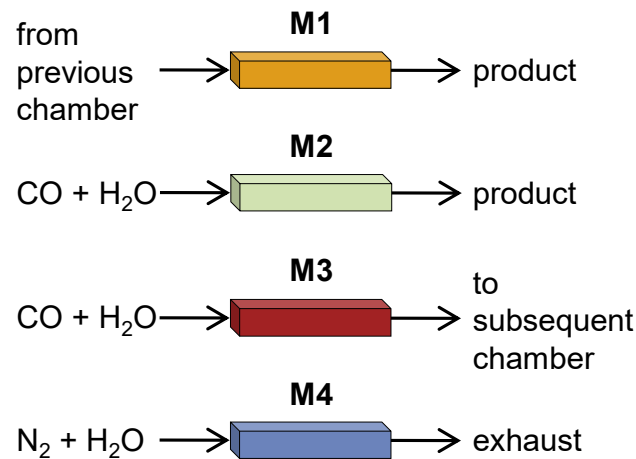


Figure 8. Process operation modes. M1: feed from previous chamber, outlet product; M2: reaction feed, outlet product; M3: reaction feed, outlet to subsequent chamber; M4: regeneration feed, outlet exhaust.

A typical operation scheme is depicted in Figure 9a for the first 900 s for all chambers. According to the operational concept, the interconnected chambers in M1 and M3 are dependent on each other. The resulting time span for M4 is the limiting factor for the sorbent regeneration. As always one chamber is either in M1 or M2, a constant product gas flow is ensured, and a nearly CO_2 -free product flow leaves the reactor. Figure 9b shows the H_2 volume fraction in the product flow of the total reactor (six chambers) and of chamber 1. The H_2 volume fraction approaches a constant value of about 0.62 after the first cycle; the rest of the product gas flow consists of inert N_2 and unreacted H_2O .

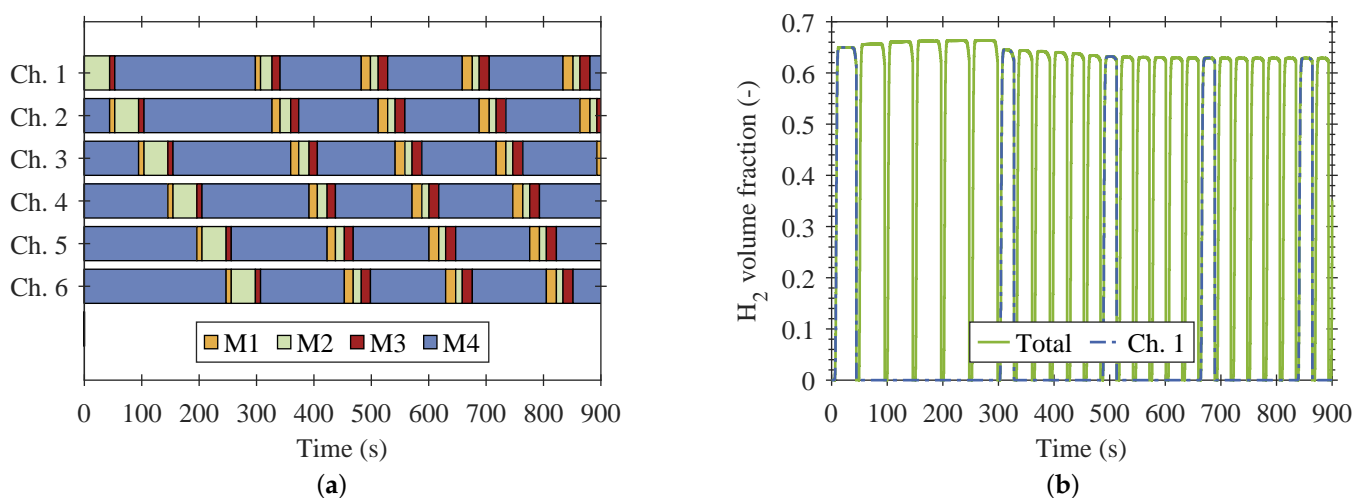


Figure 9. (a) Operation scheme for six reaction chambers, and (b) H_2 volume fraction in the product for all chambers combined ("total") and for chamber 1 for the first 900 s. Switching condition M2 to M3: CO_2 volume fraction in product > 0.05 ; M3 to M4: CO_2 volume fraction to subsequent chamber > 0.2 .

The time span in which a chamber stays in each mode and the resulting sorbent loading at the end of each mode as a function of the cycle number is shown for chamber 1 in Figure 10. The relative sorbent loading refers to the maximum loading after 400 s reactive adsorption. A significant reduction of the cycle time span by almost 50% is visible after the first cycle. Due to the limited regeneration time, the initial time span of reactive adsorption can no longer be reached in subsequent cycles, as the sorbent cannot be fully regenerated. After the third cycle, the time spans for the different modes as well as the relative sorbent loadings approach constant values. Hence, the overall system is operating in steady-state. The interconnection of two subsequent chambers in M3 and M1 allows for an increased sorbent usage from 72.6% (at the end of M2) to 87.1% (at the end of M3) for the prevailing process conditions, while maintaining the CO₂ volume fraction in the product flow below 5%.

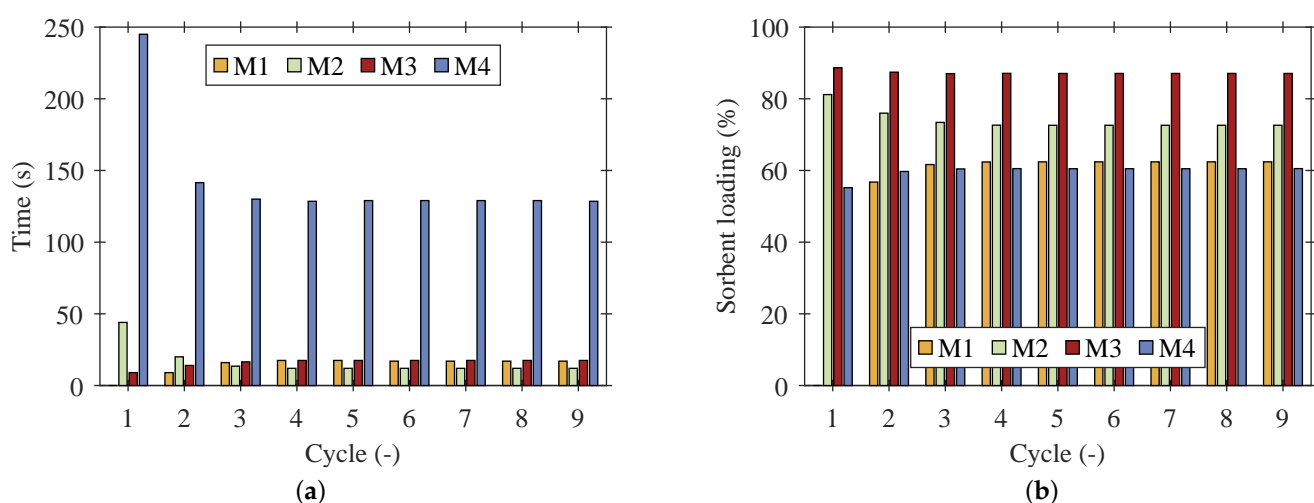


Figure 10. Cyclic operation in six reaction chambers; results shown for nine cycles in chamber 1. (a) Time span of the modes depending on the cycle number, and (b) relative sorbent loading at the end of the modes.

These results show the feasibility of the novel Matlab Simulink Stateflow implementation of the SEWGS model for process optimization. Using a Simulink implementation for a chemical reactor and utilizing Stateflow simplifies the following: simulation-driven development of operating procedures, performance evaluation of larger and more complex systems, and safe failure management. These advantages enable rapid prototyping with MATLAB code generation into programming language for automation systems (PLC) [41] and could thus simplify real plant operation.

5. Conclusions

A dynamically operated compact SEWGS reactor was modelled to optimize its operation procedure. The reactor consists of six identical reaction chambers, which are operated in cycles of reactive adsorption and desorption. The model contains coupled PDEs and is based on kinetic expressions for adsorption, reaction, and desorption.

A novel simulation approach for time- and space-dependent cyclic reactor operation was presented. This approach enables automated adjustment of switching times during runtime according to specified conditions, such as exceeding a threshold of CO₂ concentration in the product stream. For that reason, switching times do not need to be pre-defined and can be optimized dynamically.

First, the applicability of the novel method was verified by comparison with existing and well-established methods for reactive adsorption in one reaction chamber. Therefore, a base case simulation was implemented and solved with MATLAB's pdepe solver. These results were compared with those obtained via MoL (spatial discretization with FD and

ODE system solution with MATLAB's ode15s solver) to determine the required number of spatial discretization cells and to justify the discretization scheme.

Then, the MoL equations were implemented graphically in MATLAB Simulink. Only minor deviations between the results of all methods verify the discretization and suggest the reliability of the MoL implementation in Simulink.

Finally, the basic model was expanded to a complex model distinguishing between initialization, reactive adsorption, and regeneration modes. A comprehensive data structure for reliable data handling was established. A Stateflow machine was designed to simulate automated cyclic switching between six reaction chambers for continuous synthesis gas production. Overall process modeling included a configuration of subsequent interconnected reactor chambers for optimized sorbent usage, while the CO₂ volume fraction in the product flow could still be kept below 5%. Due to automated switching between interconnected reaction chambers, an increase of sorbent usage from 72.6% to 87.1% could be elaborated in the presented case.

This case study has shown that carefully chosen operating parameters and process configurations together with simulation-driven process design can significantly enhance the exploitation of the full sorption capacity and therefore increase the efficiency of sorption-enhanced reaction processes. The novel simulation approach can serve as a practical example for dynamic reactor modeling.

Author Contributions: Conceptualization, T.J.S., methodology, T.J.S.; software, T.J.S., J.-H.K., and S.D.; validation, T.J.S., formal analysis, T.J.S., investigation, T.J.S., resources, T.J.S., data curation, T.J.S., writing—original draft preparation, T.J.S., writing—review and editing, T.J.S. and P.P.; visualization, T.J.S., supervision, P.P.; project administration, P.P.; funding acquisition, P.P. All authors have read and agreed to the published version of the manuscript.

Funding: The work presented in this paper is part of the European project Kerogreen, which has received funding from the European Union's Horizon 2020 research and innovation programme under grant agreement no. 763909.

Conflicts of Interest: The authors declare no conflict of interest.

Abbreviations

The following abbreviations are used in this manuscript:

BFDM	Backward finite difference method of first order
CFDM	Centered finite difference method of second order
Ch.	Chamber
CSTR	Continuously stirred tank reactor
DAE	Differential algebraic equation
DASOLV	Implicit backward differentiation formula solver in gPROMS
DMES	Dimethyl ether synthesis
FD	Finite Difference
FEM	Finite elements method
K-HTC	K ₂ CO ₃ -promoted hydrotalcite
LDF	Linear driving force model
M1-M4	Mode 1-4
MoL	Method-of-lines
ODE	Ordinary differential equation
ode15s	Solver for stiff ODEs in MATLAB
PDE	partial differential equation
pdepe	Solver for systems of parabolic and elliptic PDEs in MATLAB
PLC	Programmable logic controller
PSA	Pressure swing adsorption
PTSA	Pressure temperature swing adsorption
SEWGS	Sorption-enhanced water–gas shift
SMR	Steam-methane reforming
TSA	Temperature swing adsorption
WGS	Water–gas shift

The following symbols are used in this manuscript:

$\beta_{j,\text{des},(i)}$	activation energy change	(J mol ⁻¹)
ε_b	bed void fraction	(-)
ε_p	particle void fraction	(-)
ν_i	stoichiometric reaction coefficient	(-)
ρ	bulk density	(kg m ⁻³)
$a_{\text{ads},i}$	adsorption rate	(mol kg ⁻¹ s ⁻¹)
c^*	pdepe diagonal matric	(-)
c_i	bulk phase concentration	(mol m ⁻³)
\bar{c}_i	particle void phase concentration	(mol m ⁻³)
$D_{\text{ax},i}$	axial dispersion coefficient	(m ² s ⁻¹)
$D_{\text{eff},i}$	effective diffusion coefficient	(m ² s ⁻¹)
$D_{\text{mix},i}$	gas mixture diffusion coefficient	(m ² s ⁻¹)
E_a	activation energy	(J mol ⁻¹)
eq	equilibrium	(-)
f^*	pdepe flux term coefficient	(-)
F_{STP}	volumetric flow rate at STP	(ml min ⁻¹)
h	slit height	(mm)
$\Delta H_{\text{R}}^{\ominus}$	standard reaction enthalpy	(kJ mol ⁻¹)
i	species CO, H ₂ O, CO ₂ , H ₂ , N ₂	(-)
j	sorption site A, B, C	(-)
$k_{\text{C,rep1}}$	exchange rate coefficient 1	(bar ⁻¹ s ⁻¹)
$k_{\text{C,rep2}}$	exchange rate coefficient 2	(bar ⁻¹ s ⁻¹)
K_{eq}	equilibrium constant	(-)
k_j	Freundlich adsorption coefficient	(mol kg ⁻¹ bar ⁻¹)
$k_{j,\text{ads}}$	adsorption coefficient	(s ⁻¹)
$k_{j,\text{des},(i)}$	desorption coefficient	(s ⁻¹)
$k_{j,\text{des},(i)}^1$	desorption coefficient	(s ⁻¹)
$k_{\text{LDF},i}$	linear driving force coefficient	(s ⁻¹)
k_{∞}	frequency factor	(mol bar ⁻² g ⁻¹ h ⁻¹)
l	slit length	(mm)
m	tiny value exponent	(-)
m^*	pdepe symmetry constant	(-)
n	index variable	(-)
N	number of cells	(-)
n_j	Freundlich adsorption intensity	(-)
O	approximation error	(-)
p^*	pdepe boundary coefficient	(-)
$p_{(i)}$	(partial) pressure	(bar)
q^*	pdepe boundary coefficient	(-)
$q_{j,i}$	sorbent loading of species i on site j	(mol kg ⁻¹)
r_p	particle radius	(m)
r_{WGS}	WGS reaction rate	(mol kg ⁻¹ s ⁻¹)
R	gas constant	(J mol ⁻¹ K ⁻¹)
s^*	pdepe source term coefficient	(-)
t	time	(s)
T	temperature	(K)
u	gas velocity	(m s ⁻¹)
v	dependent variable	(-)
w	slit width	(mm)
w_{cat}	catalyst weight fraction	(-)
y_i	volume fraction	(-)
z	axial coordinate	(m)

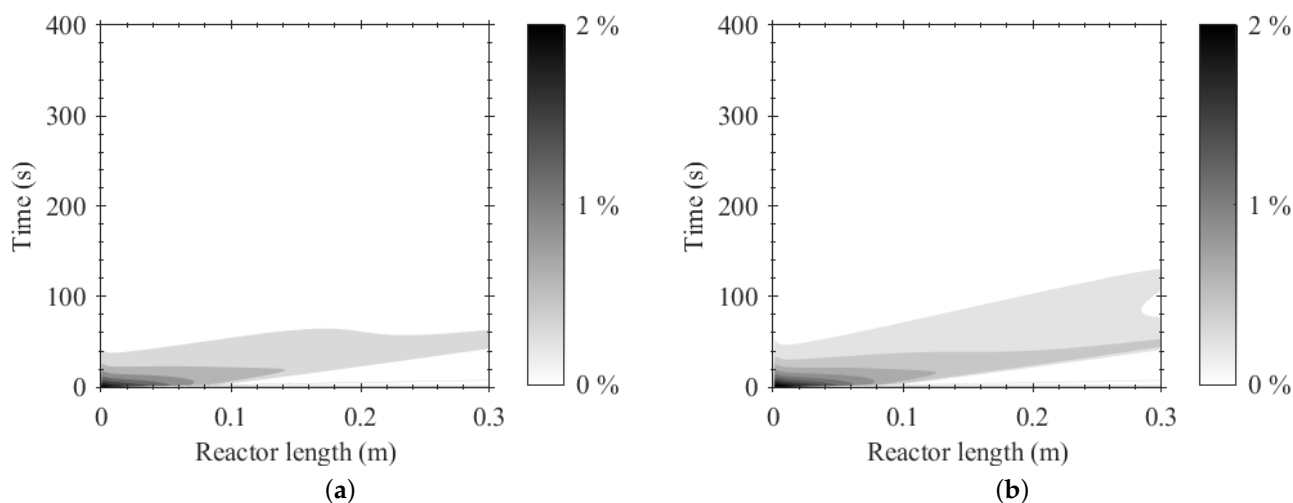
Appendix A

Table A1. Kinetic coefficients. Adapted from [28,29].

Adsorption / Desorption	
$k_{A,ads}$	$4.18 \times 10^{-2} \text{ s}^{-1}$
k_A	$1.69 \text{ mol kg}^{-1} \text{ bar}^{-1}$
n_A	0.235
$k_{A,des}^1$	$7.84 \times 10^{-9} \text{ s}^{-1}$
$\beta_{A,des}$	$1.72 \times 10^5 \text{ J mol}^{-1}$
$k_{B,ads}$	$9.29 \times 10^{-2} \text{ s}^{-1}$
k_B	$0.31 \text{ mol kg}^{-1} \text{ bar}^{-1}$
n_B	0.239
$k_{B,des}^1$	$4.41 \times 10^{-5} \text{ s}^{-1}$
$\beta_{B,des}$	$6.27 \times 10^4 \text{ J mol}^{-1}$
$k_{C,ads}$	$0.1 \text{ bar}^{-1} \text{ s}^{-1}$
$k_{C,rep1}$	$5.0 \times 10^{-3} \text{ bar}^{-1} \text{ s}^{-1}$
$k_{C,rep2}$	$1.4 \times 10^{-2} \text{ bar}^{-1} \text{ s}^{-1}$
k_{C,des,H_2O}^1	$5.23 \times 10^{-11} \text{ s}^{-1}$
k_{C,des,CO_2}^1	$2.06 \times 10^{-10} \text{ s}^{-1}$
β_{C,des,H_2O}	$5.41 \times 10^4 \text{ J mol}^{-1}$
β_{C,des,CO_2}	$5.00 \times 10^4 \text{ J mol}^{-1}$
m	1×10^{-16}
WGS Reaction	
k_∞	$2.96 \times 10^5 \text{ mol bar}^{-2} \text{ g}^{-1} \text{ h}^{-1}$
E_a	$47.400 \text{ J mol}^{-1}$

Table A2. Computation time for pdepe and MoL simulations for reactive adsorption in one reaction chamber.

Number of Cells (-)	MoL						pdepe
	10	30	50	100	200	250	3000
Computation Time (min)	0.04	0.22	0.27	4.96	46.81	90.93	12.19

Figure A1. Time and space-dependent deviation from molar balance for reactive adsorption in one reaction chamber: (a) pdepe, and (b) MoL ($N = 100$) simulation results.

References

1. UN. COP26 Outcomes. In Proceedings of the UN Climate Change Conference at the SEC, Glasgow, UK, 31 October–13 November 2021.
2. United Nations/Framework Convention on Climate Change. Adoption of the Paris Agreement. In Proceedings of the 21st Conference of the Parties, Paris, France, 30 November–11 December 2015.
3. European Commission. *A European Strategy for Low-Emission Mobility*; EEA: Copenhagen, Denmark, 2020.
4. Goede, A.P.H. CO₂ neutral fuels. *EPJ Web Conf.* **2018**, *189*, 00010. [[CrossRef](#)]
5. Rodrigues, A.E.; Madeira, L.M.; Wu, Y.J.; Faria, R. Sorption enhanced reaction processes. In *Sustainable Chemistry Series*; World Scientific: New Jersey, NJ, USA, 2018; Volume 1.
6. Lee, C.H.; Lee, K.B. Application of one-body hybrid solid pellets to sorption-enhanced water gas shift reaction for high-purity hydrogen production. *Int. J. Hydrogen Energy* **2014**, *39*, 18128–18134. [[CrossRef](#)]
7. Soria, M.A.; Rocha, C.; Tosti, S.; Mendes, A.; Madeira, L.M. CO_x free hydrogen production through water-gas shift reaction in different hybrid multifunctional reactors. *Chem. Eng. J.* **2019**, *356*, 727–736. [[CrossRef](#)]
8. Stadler, T.J.; Barbig, P.; Kiehl, J.; Schulz, R.; Klövekorn, T.; Pfeifer, P. Sorption-Enhanced Water-Gas Shift Reaction for Synthesis Gas Production from Pure CO: Investigation of Sorption Parameters and Reactor Configurations. *Energies* **2021**, *14*, 355. [[CrossRef](#)]
9. Zhu, X.; Li, S.; Shi, Y.; Cai, N. Recent advances in elevated-temperature pressure swing adsorption for carbon capture and hydrogen production. *Prog. Energy Combust. Sci.* **2019**, *75*, 100784. [[CrossRef](#)]
10. Harrison, D.P. Sorption-Enhanced Hydrogen Production: A Review. *Ind. Eng. Chem. Res.* **2008**, *47*, 6486–6501. [[CrossRef](#)]
11. Gazzani, M.; Macchi, E.; Manzolini, G. CO₂ capture in integrated gasification combined cycle with SEWGS—Part A: Thermodynamic performances. *Fuel* **2013**, *105*, 206–219. [[CrossRef](#)]
12. Schiesser, W.E. *A Compendium of Partial Differential Equation Models: Method of Lines Analysis with MATLAB*; Cambridge University Press: Cambridge, UK, 2009.
13. Lee, K.B.; Verdooren, A.; Caram, H.S.; Sircar, S. Chemisorption of carbon dioxide on potassium-carbonate-promoted hydrotalcite. *J. Colloid Interface Sci.* **2007**, *308*, 30–39. [[CrossRef](#)]
14. Reijers, H.T.J.; Boon, J.; Elzinga, G.D.; Cobden, P.D.; Haije, W.G.; van den Brink, R.W. Modeling Study of the Sorption-Enhanced Reaction Process for CO₂ Capture. I. Model Development and Validation. *Ind. Eng. Chem. Res.* **2009**, *48*, 6966–6974. [[CrossRef](#)]
15. Najmi, B.; Bolland, O.; Colombo, K.E. A systematic approach to the modeling and simulation of a Sorption Enhanced Water Gas Shift (SEWGS) process for CO₂ capture. *Sep. Purif. Technol.* **2016**, *157*, 80–92. [[CrossRef](#)]
16. Karagöz, S.; Tsotsis, T.T.; Manousiouthakis, V.I. Multi-scale modeling and simulation of a novel membrane reactor (MR)/adsorptive reactor (AR) process. *Chem. Eng. Process. Process. Intensif.* **2019**, *137*, 148–158. [[CrossRef](#)]
17. Di Giuliano, A.; Gallucci, K.; Giancaterino, F.; Courson, C.; Foscolo, P.U. Multicycle sorption enhanced steam methane reforming with different sorbent regeneration conditions: Experimental and modelling study. *Chem. Eng. J.* **2019**, *377*, 119874. [[CrossRef](#)]
18. van Kampen, J.; Boon, J.; Vente, J.; van Sint Annaland, M. Sorption enhanced dimethyl ether synthesis for high efficiency carbon conversion: Modelling and cycle design. *J. CO₂ Util.* **2020**, *37*, 295–308. [[CrossRef](#)]
19. Guffanti, S.; Visconti, C.G.; van Kampen, J.; Boon, J.; Groppi, G. Reactor modelling and design for sorption enhanced dimethyl ether synthesis. *Chem. Eng. J.* **2021**, *404*, 126573. [[CrossRef](#)]
20. Guffanti, S.; Visconti, C.G.; Groppi, G. Model Analysis of the Role of Kinetics, Adsorption Capacity, and Heat and Mass Transfer Effects in Sorption Enhanced Dimethyl Ether Synthesis. *Ind. Eng. Chem. Res.* **2021**, *60*, 6767–6783. [[CrossRef](#)]
21. Jang, H.M.; Lee, K.B.; Caram, H.S.; Sircar, S. High-purity hydrogen production through sorption enhanced water gas shift reaction using K₂CO₃-promoted hydrotalcite. *Chem. Eng. Sci.* **2012**, *73*, 431–438. [[CrossRef](#)]
22. Aloisi, I.; Di Giuliano, A.; Di Carlo, A.; Foscolo, P.U.; Courson, C.; Gallucci, K. Sorption enhanced catalytic Steam Methane Reforming: Experimental data and simulations describing the behaviour of bi-functional particles. *Chem. Eng. J.* **2017**, *314*, 570–582. [[CrossRef](#)]
23. Zheng, Y.; Shi, Y.; Li, S.; Yang, Y.; Cai, N. Elevated temperature hydrogen/carbon dioxide separation process simulation by integrating elementary reaction model of hydrotalcite adsorbent. *Int. J. Hydrogen Energy* **2014**, *39*, 3771–3779. [[CrossRef](#)]
24. Boon, J.; Cobden, P.D.; van Dijk, H.; van Sint Annaland, M. High-temperature pressure swing adsorption cycle design for sorption-enhanced water—Gas shift. *Chem. Eng. Sci.* **2015**, *122*, 219–231. [[CrossRef](#)]
25. Stankiewicz, A.I.; Moulijn, J.A. Process intensification: Transforming chemical engineering. *Chem. Eng. Prog.* **2000**, *96*, 22–34.
26. Keil, F.J. Process intensification. *Rev. Chem. Eng.* **2018**, *34*, 135–200. [[CrossRef](#)]
27. Di Giuliano, A.; Pellegrino, E. Numerical integration strategies of PFR dynamic models with axial dispersion and variable superficial velocity: the case of CO₂ capture by a solid sorbent. *Heliyon* **2019**, *5*, e02040. [[CrossRef](#)] [[PubMed](#)]
28. Choi, Y.; Stenger, H.G. Water gas shift reaction kinetics and reactor modeling for fuel cell grade hydrogen. *J. Power Sources* **2003**, *124*, 432–439. [[CrossRef](#)]
29. Coenen, K.; Gallucci, F.; Hensen, E.; van Sint Annaland, M. Kinetic model for adsorption and desorption of H₂O and CO₂ on hydrotalcite-based adsorbents. *Chem. Eng. J.* **2019**, *355*, 520–531. [[CrossRef](#)]
30. Moe, J.M. Design of water-gas shift reactors. *Chem. Eng. Prog.* **1962**, *58*, 8.
31. Poling, B.E.; Prausnitz, J.M.; O'Connell, J.P. *The Properties of Gases and Liquids*, 5th ed.; McGraw-Hill: New York, NY, USA, 2001.
32. Yang, R.T. *Gas Separation by Adsorption Processes*; Butterworths series in chemical engineering; Butterworths: Boston, MA, USA, 1987.
33. MathWorks. Solve 1-D parabolic and elliptic PDEs—MATLAB pdepe. Available online: <https://de.mathworks.com/help/matlab/ref/pdepe.html> (accessed on 19 January 2022).

34. Skeel, R.D.; Berzins, M. A Method for the Spatial Discretization of Parabolic Equations in One Space Variable. *SIAM J. Sci. Stat. Comput.* **1990**, *11*, 1–32. [[CrossRef](#)]
35. Shampine, L.F.; Reichelt, M.W. The Matlab ODE suite. *SIAM J. Sci. Comput.* **1997**, *18*, 1–22. [[CrossRef](#)]
36. Ukrainczyk, N.; Koenders, E.A.B. Numerical Model for Chloride Ingress in Cement Based Materials: Method of Lines Implementation for Solving Coupled Multi-species Diffusion with Binding. *Comput. Mater. Civ. Eng.* **2016**, *1*, 109–119.
37. MathWorks. Simulink Product Description—MATLAB & Simulink. Available online: <https://de.mathworks.com/help/simulink/gs/product-description.html> (accessed on 19 January 2022).
38. Puente León, F.; Jäkel, H. *Signale und Systeme*, 7th ed.; De Gruyter Studium, De Gruyter Oldenbourg: Berlin, Germany; Boston, MA, USA, 2019.
39. MathWorks. Choose a Solver—MATLAB & Simulink. Available online: <https://de.mathworks.com/help/simulink/ug/choose-a-solver.html> (accessed on 19 January 2022).
40. MathWorks. Overview of Stateflow Objects—MATLAB & Simulink. Available online: <https://de.mathworks.com/help/stateflow/ug/overview-of-stateflow-objects.html> (accessed on 19 January 2022).
41. Bayrak, G.; Abrishamchian, F.; Vogel-Heuser, B. Effiziente Steuerungsprogrammierung durch automatische Modelltransformation von Matlab/Simulink/Stateflow nach IEC 61131-3. *Autom. Prax.* **2008**, *50*, 49–55.